A semi-analytical numerical method for modelling the normal wheel–rail contact

Aquib Qazi, Honoré Yin, Michel Sebès, Hugues Chollet, Cédric Pozzolini

A semi-analytical numerical method for modelling the normal wheel-rail contact

Aquib Qazi[a,b,c], Honoré Yin[b], Michel Sebès[a], Hugues Chollet[a] & Cédric Pozzolini[c]

[a] COSYS-GRETTIA, Univ Gustave Eiffel, IFSTTAR, Marne-la-Vallée, France
[b] Laboratoire Navier, École des Ponts ParisTech, Univ Gustave Eiffel, CNRS, Marne-la-Vallée, France
[c] ESI Group, France

ARTICLE HISTORY
This is an original manuscript of an article published by Taylor & Francis in Vehicle System Dynamics on 1st December 2020, available online: https://doi.org/10.1080/00423114.2020.1854319

ABSTRACT
A new semi-analytical boundary element method is proposed for determining the wheel-rail contact zone and the normal stress distribution within it. The potential contact area is discretised using strip elements, employing an iterative algorithm to satisfy the contact constraints. At each iteration, the length of the contact strips is updated using an analytical expression based on Hertz's theory. This simplified formulation provides good approximation of the pressure distribution and consequently the contact area in non-elliptic cases. The reduction in the number of system unknowns by using a semi-analytical methodology also enables fast computation speeds, an indispensable requirement in railway dynamics.

KEYWORDS
wheel-rail contact; Hertz; non-elliptic contact; vehicle dynamics; contact mechanics; boundary element method

1. Introduction

Safety, track fatigue analyses, and maintenance of railway vehicles are only some of the applications that highlight the importance of wheel-rail contact models. The complexity of different operations necessitates very different levels of modelling: a simplified and coarse model may often be sufficient. For hardware-in-the-loop simulations, where the calculations must be carried out in real time over railway tracks which are several kilometres long, very approximate wheel-rail contact models are generally used. Conversely, other applications require more sophisticated models, such as in the estimation of wear in urban rail networks, or the assessment of rolling contact fatigue. The shape of the contact area and the stress distribution within it categorise the different normal contact models available in the literature [1–4].

The case of normal contact between two continuous and non-conforming bodies was first treated by Hertz in 1882 [5], assuming frictionless contact and each solid body as an elastic half-space. The Hertzian solution is characterised by an elliptical contact

CONTACT Aquib Qazi Email: aquib.qazi@univ-eiffel.fr

patch, with a semi-ellipsoidal normal pressure distribution acting within the contact area. This approach is limited to profiles with constant curvature, and therefore may lead to approximate results in railway applications where the curvature of the profiles changes along the width of the rail section.

The use of discrete methods offers a more realistic approximation of the contact conditions in real-life applications. The finite element method (FEM) has already been used in various studies for elasto-plastic stress analyses and creep force characteristics, employing both implicit and explicit approaches [6,7]. Certain recent works have also used Nitsche's method for frictional contact problems as opposed to the classical penalty methods or mixed methods, which offers good convergence and robustness [8]. Variational methods as the one described by Kalker's complete theory [9] and implemented in the program CONTACT [10], the boundary element method (BEM) like the one presented by Knothe and Le The [11], or the matrix inversion method (MIM) by Johnson [12] also enable a good estimation of the contact properties. Despite the advances in computational prowess in recent years, discrete methods continue to struggle in terms of their capability to be used online in vehicle dynamics simulations. A very fine discretisation is usually required with FEM approaches to satisfactorily represent the contact patch boundaries, while classical boundary element methods require iterative techniques over large potential contact grids to verify the stress constraints.

In most software applications, a compromise is reached between the level of accuracy that is deemed acceptable and the time it takes to solve the contact problem. This has given rise to an intermediate level of approximate methods based on the theory of virtual penetration of the contacting surfaces such as the Linder model [13], the Kik-Piotrowski model [14], the semi-Hertzian model (STRIPES) [15], and the extended Kik-Piotrowski (EKP) model [16] amongst others. The contact area in these approaches is approximated using the area in which the surfaces would overlap if there is no deformation. This overlapping area is bigger than the actual contact patch, and a scaling factor is used to prescribe the virtual penetration such that the interpenetration zone approaches the real contact area. The technique used for determining the scaling parameter is what broadly differentiates these approaches [17]. There exists in parallel another family of models wherein the non-elliptical part of the contact area is approximated using a series of individual ellipses. This so-called multi-Hertzian method, proposed by Pascal and Sauvage [18], is further simplified by Ayasse et al. [19] to an analytical approach. Some of the questions raised regarding these models when compared against virtual penetration methods in [2] have been addressed recently by Pascal [20].

A proposed improvement to these models is through the introduction of an analytical approximation for the surface deformation in the method ANALYN [21]. Although the results are promising in comparison to other simplified methods, this method remains sensitive to the negative-curvature correction, a characteristic of all point-based contact models based on Hertz' theory. This makes it challenging to implement the method as a true black-box solution in dynamic vehicle simulation. It is generally noted that this approach gives a good approximation of the contact area when the pressure distribution estimated is also accurate. A better approximation of the pressure distribution using a more thorough approach in the above family of methods should lead to better estimation of the contact patch, which forms the basis of the new semi-analytical approach proposed in this article.

In the first part, a reduced formulation of the contact between two elastic half-spaces is used together with a Hertzian model to solve the normal contact, following a semi-

analytical methodology. The novel method is then validated using the results from STRIPES [15], ANALYN [21], and CONTACT [10] with theoretical as well as wheel-rail profiles. A comparison of the required computational resources is also carried out using different numerical approaches, before the final conclusions.

2. Methodology

2.1. Theoretical background

The problem describing the stress field in a semi-infinite half-space subjected to a concentrated normal surface force was studied in detail by Boussinesq [22]. For the half-space consideration to be valid locally, the contact area dimensions must be significantly smaller as compared to the principal radii of the contacting surfaces. This is generally true when considering several common contact scenarios such as the tread contact between wheels and rails. The following assumptions are also made:

- The bodies are elastic, homogeneous and isotropic.
- The contacting surfaces have a continuous profile.
- The normal and tangential problems can be solved sequentially.

One possible solution is using the potential theory of Boussinesq [22], described exhaustively in the book by Johnson [12]. The normal elastic displacement $\bar{u}(x, y)$ is related to the normal pressure distribution $p(x, y)$ by the integral equation [23]

$$\forall (x, y) \in \Sigma, \quad \bar{u}(x, y) = \iint_{\Sigma_c} p(\xi, \eta) T(x, y; \xi, \eta) d\xi d\eta, \tag{1}$$

where Σ is the half-space domain under consideration, Σ_C is the zone of the contact, and T is Boussinesq's influence function defined as

$$\forall (x, y; \xi, \eta) \in \Sigma^2, \quad T(x, y; \xi, \eta) = \frac{1}{\pi E^\star} \frac{1}{\sqrt{(x-\xi)^2 + (y-\eta)^2}}. \tag{2}$$

$E^\star$ is the effective Young's modulus of elasticity for the two contacting bodies Ω_1 and Ω_2 such that

$$\frac{1}{E^\star} = \left(\frac{1 - \nu_1^2}{E_1} + \frac{1 - \nu_2^2}{E_2} \right), \tag{3}$$

where E_1 and E_2 are the modulus of elasticity, while ν_1 and ν_2 are the Poisson's ratios for the two solids. With a defined rigid approach δ, the only geometrical input required to solve the contact problem is the separation between the two undeformed surfaces $h(x, y)$. The normal surface deformation $\bar{u}(x, y) = \bar{u}_1(x, y) + \bar{u}_2(x, y)$ must be evaluated at each point within the contact zone. This contact problem can be summarised in Figure 1. Considering Σ_C as the area of contact, the conditions of Signorini give the cases of separation and of contact:

$$\forall (x, y) \notin \Sigma_C, \quad \delta - \bar{u}(x, y) - h(x, y) < 0 \text{ and } p(x, y) = 0, \tag{4}$$

$$\forall (x, y) \in \Sigma_C, \quad \delta - \bar{u}(x, y) - h(x, y) = 0 \text{ and } p(x, y) > 0. \tag{5}$$

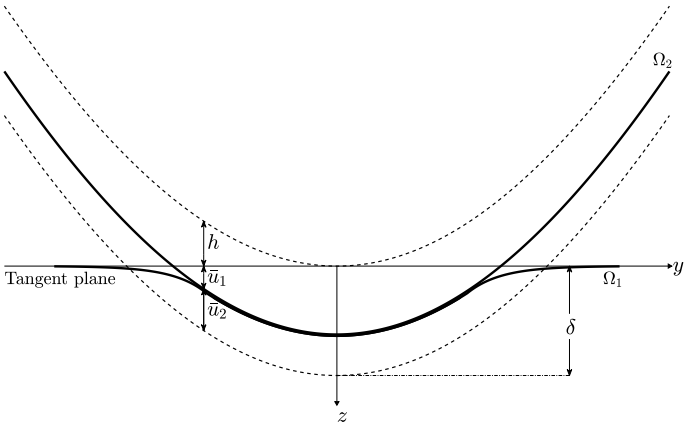

Figure 1. Two elastic bodies in contact

The boundary conditions defined in Equations (4) and (5) ensure that the normal pressure can only act within the contact zone, vanishing at the boundary of the contact area. The two bodies are also prevented from interpenetrating. If the rigid approach δ is given, the problem to be solved can be completely described by Equations (1) and (5). If the total resultant force N is known in advance, the following equilibrium condition is added:

$$\forall (x, y) \in \Sigma_C, \qquad N = \iint_{\Sigma_c} p(\xi, \eta) d\xi d\eta. \tag{6}$$

2.2. Towards a reduced approach

The classical direct method to solve the contact problem is the matrix inversion method (MIM) found in [12]. The potential contact area in the boundary element problem is overestimated in both the lateral and the rolling directions and divided into a rectangular grid, wherein the contact constraints of Equations (4) and (5) are then evaluated. The elements in which the pressure distribution has negative values are discarded, and the procedure is repeated until all the remaining elements satisfy the boundary conditions. The elastic deformation is thus calculated at each iteration for each element within the potential contact area, resulting in a large expenditure of computational resources. In the proposed new approach, the pressure distribution is assumed to be symmetric and elliptic about the $x = 0$ plane and the potential area of contact is discretised only in the lateral y direction. A similar strategy for discretisation is also used by Reusner for the treatment of roller bearings in [24], and by Knothe and Le–The for more arbitrary elastic bodies in [11]. The novel approach in the present paper is to consider the contact patch boundaries as a quasi-known quantity dependent on the form of the normal stress distribution. The potential contact area is first divided into thin strips with the larger dimension in the rolling direction, as shown in Figure 2, from where the name MIM-1D is chosen for the new method. The unknown in this case reduces to the maximum pressure values p_{0_i} at the centre of each strip i. At each iteration, the half-length of the contact strip a_i in the rolling direction is then computed as a function of the maximum pressure distribution p_{0_i}, using an approximate analytical formulation based on Hertz' theory.

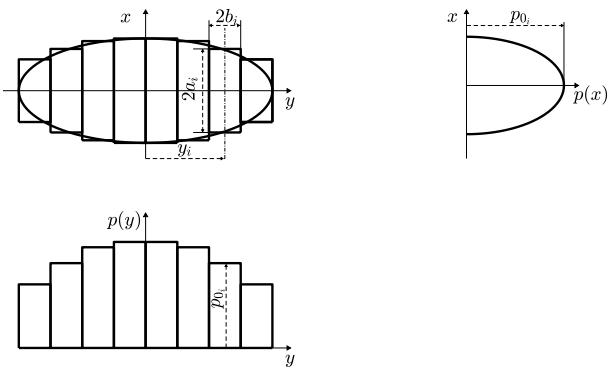

Figure 2. Contact area Σ_C divided into strips, and the normal pressure distribution [11]

2.3. Discrete problem

The half-length and the half-width of each strip element are given as a_i and b_i respectively. The pressure distribution over each strip is assumed to be semi-elliptical in the x direction, and constant in the y direction. Thus, the expression for the pressure distribution over each strip may be written as

$$p(x, y_i) = p_{0_i} \sqrt{1 - \left(\frac{x}{a_i}\right)^2}, \tag{7}$$

where p_{0_i} is the maximum pressure at the centre (x_i, y_i) of the strip i. The deformation and the separation at the centre are denoted as u_i and h_i respectively. Equations (1) and (5) in discrete form are:

$$\forall i \in [1, n], \qquad u_i = \sum_{j=1}^{n} C_{ij} p_{0_j}, \tag{8}$$

$$\forall i \in [1, n] \ni (x_i, y_i) \in \Sigma_C, \qquad \delta - u_i - h_i = 0 \text{ and } p_{0_i} > 0, \tag{9}$$

where n denotes the total number of elements in the potential contact area. The terms C_{ij} from Equation (8) are called the coefficients of influence, and are defined as

$$C_{ij} = \frac{2}{\pi E^\star} \int_{y_j - b_j}^{y_j + b_j} \int_0^{a_j} \frac{\sqrt{1 - (\frac{\xi}{a_j})^2}}{\sqrt{(x_i - \xi)^2 + (y_i - \eta)^2}} d\xi d\eta. \tag{10}$$

The expression for C_{ij} describes the influence of normal stress distribution in the jth element to induce elastic displacement in the ith element. The x_i terms are ignored as they always remain zero in the case of MIM-1D. Equation (10) is written as:

$$C_{ij} = \frac{2}{\pi E^\star} \left[\int_{y_j - b_j}^{y_j + b_j} \int_0^{a_j} \frac{\sqrt{1 - (\frac{\xi}{a_j})^2} - 1}{\sqrt{\xi^2 + (y_i - \eta)^2}} d\xi d\eta + \int_{y_j - b_j}^{y_j + b_j} \int_0^{a_j} \frac{d\xi d\eta}{\sqrt{\xi^2 + (y_i - \eta)^2}} \right]. \tag{11}$$

The first integral is regular and can be evaluated numerically using Gaussian quadrature. A higher number of integration points may be chosen closer to the diagonal terms. The second integral is singular when the denominator approaches zero. This expression represents the case of uniform normal pressure acting on a rectangular area of $2a_i \times 2b_i$, and an analytical solution of this problem has been presented in detail by Love [12,25]. We have

$$\begin{aligned} 2\int_{y_j-b_j}^{y_j+b_j}\int_0^{a_j} \frac{d\xi d\eta}{\sqrt{\xi^2+(y_i-\eta)^2}} = \quad & (y+b_j)\log\left[\frac{a_j+\sqrt{(y+b_j)^2+a_j^2}}{-a_j+\sqrt{(y+b_j)^2+a_j^2}}\right] \\ & + (y-b_j)\log\left[\frac{-a_j+\sqrt{(y-b_j)^2+a_j^2}}{a_j+\sqrt{(y-b_j)^2+a_j^2}}\right] \\ & + 2a_j \quad \log\left[\frac{(y+b_j)+\sqrt{(y+b_j)^2+a_j^2}}{(y-b_j)+\sqrt{(y-b_j)^2+a_j^2}}\right], \end{aligned} \tag{12}$$

where

$$y = y_i - y_j.$$

An additional advantage of treating the original integral expression in such a manner is the introduction of an analytical solution into the numerical results, which may consequently reduce the integration error linked to the quadrature method. This also permits the use of lesser number of integration points, and consequently faster calculation times. Equation (8) in matrix form is written as

$$\mathbf{u} = \mathbf{C}\ \mathbf{p}, \tag{13}$$

where the vectors $\mathbf{p}$ and $\mathbf{u}$ are given as $\{p_{0_1}, ..., p_{0_n}\}^T$ and $\{\delta - h_1, ..., \delta - h_n\}^T$ respectively. The matrix of influence coefficients $\mathbf{C}$ is

$$\mathbf{C} = \begin{bmatrix} C_{11} & \dots & C_{1n} \\ \vdots & \ddots & \vdots \\ C_{n1} & \dots & C_{nn} \end{bmatrix}. \tag{14}$$

This is the method of resolution generally followed in the case where the rigid approach δ is known in advance. Unlike in the classical method, $\mathbf{C}$ needs to be evaluated at the beginning of each iteration as the size of the elements in the x direction does not remain the same.

In the case where the normal force is prescribed instead of rigid body approach δ, the normal contact problem is solved with an additional iteration for δ. The resultant force at the end of each iteration is calculated using Equation (6):

$$N = \pi \sum_{i=1}^{n} (a_i b_i) p_{0_i}. \tag{15}$$

The initial value of δ can be taken as the Hertzian rigid body approach. The subsequent values of δ may be evaluated using a dichotomy or an iterative scheme based on Hertz' relations [11]:

$$\delta^{(m+1)} = \delta^{(m)} \left[\frac{N}{\tilde{N}^{(m)}} \right]^{\frac{2}{3}}, \tag{16}$$

where $\tilde{N}^{(m)}$ represents the resultant normal force at the end of mth iteration.

For numerical simulations, it is also possible to modify Equation (13) using the normal force over each strip N_i (see Appendix A).

2.4. Calculation of the contact patch half-length a_i

The half-length of the contact patch a_i is evaluated analytically, using the expressions from Hertz' theory locally. a_i is updated at each iteration to define the new potential contact zone, which is then used to construct the matrix $\mathbf{C}$. The equation for the Hertzian contact ellipse is

$$\left(\frac{x}{a_0} \right)^2 + \left(\frac{y}{b_0} \right)^2 = 1, \tag{17}$$

where a_0 and b_0 are the semi-axes of the ellipse [26]:

$$a_0 = m \left[\frac{3}{2} N \frac{1}{2E^\star} \frac{1}{(A+B)} \right]^{\frac{1}{3}}, \tag{18}$$

$$b_0 = n \left[\frac{3}{2} N \frac{1}{2E^\star} \frac{1}{(A+B)} \right]^{\frac{1}{3}}. \tag{19}$$

Here, A and B are the relative curvatures in the longitudinal and lateral directions respectively, while m and n are the non-dimensional Hertzian coefficients assessed using the curvatures (see Appendix in [15], or [26]). The normal pressure distribution $p(x, y)$ over the contact area is semi-ellipsoidal, and given by

$$p(x,y) = p_{0_H} \sqrt{1 - \left(\frac{x}{a_0} \right)^2 - \left(\frac{y}{b_0} \right)^2}, \tag{20}$$

with the maximum normal pressure at the centre of ellipse,

$$p_{0_H} = \frac{3}{2} \frac{N}{\pi a_0 b_0}. \tag{21}$$

Equation (17) over each strip can be written as

$$\left(\frac{a_i}{a_0} \right)^2 + \left(\frac{y}{b_0} \right)^2 = 1. \tag{22}$$

Combining Equations (20) and (22), the normal pressure distribution in the longitudinal x direction for the ith strip is

$$p(x, y_i) = p_{0_H} \frac{a_i}{a_0} \sqrt{1 - \left(\frac{x}{a_i}\right)^2}. \tag{23}$$

Comparing Equations (7) and (23), it is possible to deduce

$$p_{0_i} = p_{0_H} \frac{a_i}{a_0} = \frac{3}{2} \frac{N}{\pi a_0 b_0} \frac{a_i}{a_0}. \tag{24}$$

Using the expressions for the semi-axes a_0 and b_0 defined previously, the contact patch half-length can be found using

$$a_i = \frac{\pi}{2E^*} \frac{m^2 n}{A + B} p_{0_i}. \tag{25}$$

This Hertzian expression for the contact patch boundary depends on the geometric properties of the profiles in contact, and the normal pressure at the centre of the strip under consideration. In non-elliptic cases, the curvatures and the Hertzian coefficients are replaced by their local values. Thus,

$$a_i = \frac{\pi}{2E^*} \frac{m_i^2 n_i}{A_i + B_i} p_{0_i}. \tag{26}$$

The same expression for a_i can also be obtained using the theory of ANALYN (see Appendix B). Hertz' solution remains valid only for positive values of B_i. If the lateral curvature is negative at a given point, a correction must be carried out. Moreover, if the curvature is discontinuous, a smoothing is also applied. This correction and smoothing is done using the procedure described in [15].

2.5. Iterative resolution

Equation (26) is incorporated into the iterative algorithm presented in Figure 3 to solve the contact problem described by Equation (13). In order to speed up the computation, the matrix of influence coefficients $\mathbf{C}$ is constructed only using the elements i where the separation h_i is less than a predefined maximum value h_{max}. When the resultant normal force N is known, the same algorithm is repeated for each value of $\delta^{(m)}$, evaluated using Equation (16). The total normal force at the mth iteration $\tilde{N}^{(m)}$ is computed using Equation (15). The algorithm in this case converges when a user defined tolerance value $\epsilon = |\tilde{N}^{(m)} - N|$ is attained.

3. Results and discussion

The proposed new approach MIM-1D is implemented as a Matlab function. The approximate surface deformation method ANALYN [21], and the virtual penetration method STRIPES [15] are also programmed using Matlab. The results from the commercial version of the program CONTACT (v20.1) [10] are used as the reference.

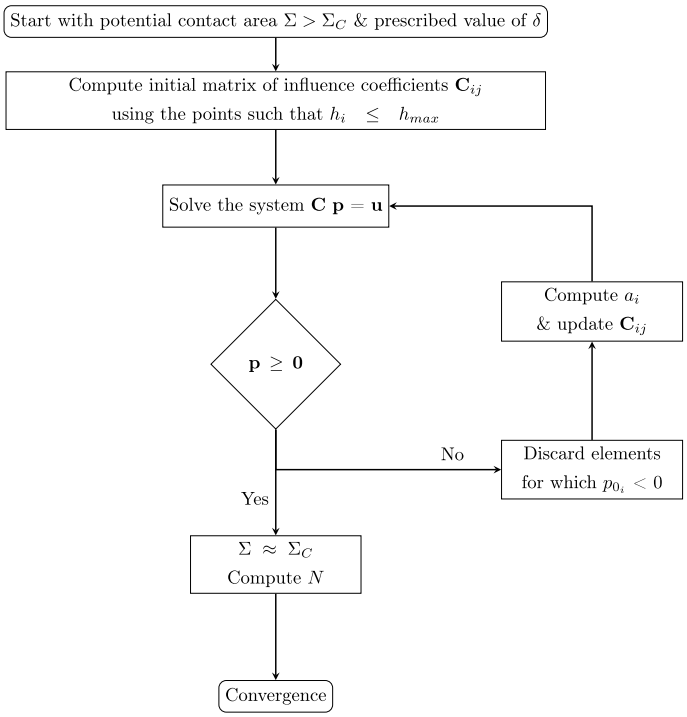

Figure 3. MIM-1D algorithm with a given rigid body approach δ

It should be noted that the ANALYN results are sensitive to the method used for the negative-curvature correction. In the original publication, the negative lateral curvature values are replaced using a fifth-degree polynomial. However, this correction strategy has not been explained in further detail, and here this is done heuristically to obtain results as close as possible to the ones presented in [21].

3.1. Theoretical profiles

3.1.1. Hertzian

To validate the new approach, a Hertzian case is considered with the contact between a sphere ($R = 40$ mm) and a flat surface. The separation curve between the two surfaces

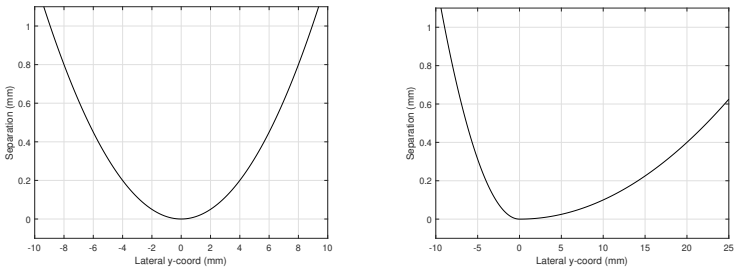

(a) Hertzian (b) Non-Hertzian

Figure 4. Separation profiles of the two contacting surfaces

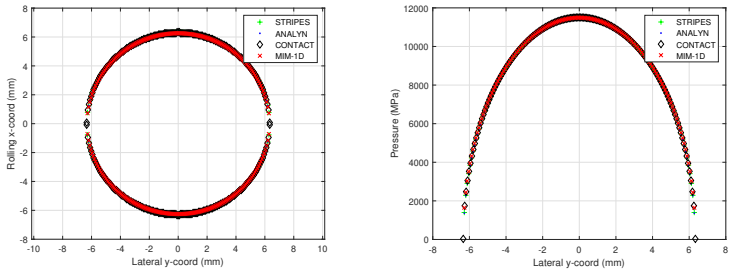

(a) Contact patch (b) Pressure distribution $p_0(y)$

Figure 5. Results for a Hertzian profile using existing methods and MIM-1D

is shown in Figure 4a. Both bodies are made of steel, with $\nu = 0.3$ and $E = 208$ GPa. The rigid approach between the two bodies is taken as 1 mm.

The contact patches obtained using different approaches and the maximum pressure distribution $p_0(y)$ are shown in Figure 5. All the methods can be observed to be in good agreement with each other. The relative error in the contact area for MIM-1D is found to be within 1% of Hertz's analytical solution, which can be attributed to the accuracy of numerical procedure used.

3.1.2. Non-Hertzian

The contact between a flat surface, and a body of revolution (rolling radius $R_n = 400$ mm) with a non-Hertzian theoretical profile developed using two different radii $R_1 = 40$ mm and $R_2 = 500$ mm on either side of the point of first contact is considered next. The separation curve between the two surfaces is shown in Figure 4b. The material properties are the same as in the Hertzian case, with the bodies pushed 1 mm towards each other.

The results for the contact area and the maximum pressure distribution are presented in Figure 6. From Figure 6a, it can be seen that MIM-1D and ANALYN correspond reasonably well with the reference results from CONTACT. The relative error in the contact area for MIM-1D is within 1% of the reference results. STRIPES notably underestimates the width of the contact patch: this is expected, as neglecting the surface deformation should lead to a smaller contact zone. Although the pressure distribution curve for ANALYN in Figure 6b follows the same trend as that of the reference, the peak of the pressure curve remains significantly higher. The results using MIM-1D can be observed to be in a better agreement with the reference method.

3.2. Wheel-rail contact

The case of wheel-rail contact is presented using the standard wheel profile S1002 over the rail profile UIC60, with an inclination of 1:40. The material for both the wheel and the rail is steel. The resultant normal contact force is taken as 78500 N. The results are presented for various positions of the wheel, displaced from its centre position over the rail, denoted by Δy. The sign convention is taken the same as in [21], where a positive Δy signifies the movement of the contact point towards the wheel flange. The discretisation size is taken as approximately 0.2 mm for all the considered cases.

The test cases are chosen to remain in the tread region with low contact angles, where the half-space assumption is not violated. From Figure 7, it can be seen the MIM-

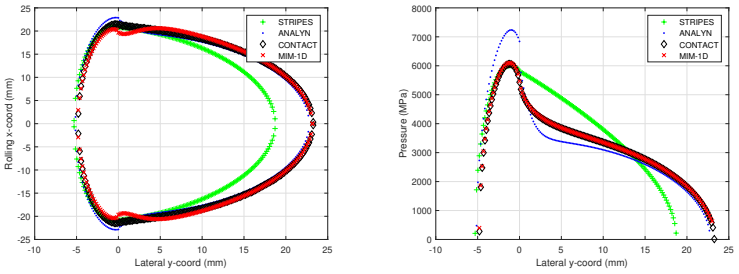

(a) Contact patch (b) Pressure distribution $p_0(y)$

Figure 6. Results for a non-Hertzian profile using existing methods and MIM-1D

1D results match closely with the reference CONTACT results in all of the presented cases. This is highlighted more prominently in the maximum pressure distribution over the contact patch length. It can also be remarked that MIM-1D manages to accurately capture the characteristic slight variations in the pressure distribution, such as those presented in the tail end of the case $\Delta y = -1$, a trait missing in the other simplified methods. ANALYN remains more precise compared to the virtual penetration methods, as neglecting the surface deformation in STRIPES again leads to an underestimated contact zone. The negative curvature compensation procedure used in STRIPES may have an effect as well [27]. This sensibility of STRIPES related to the processing of the curvature is found to be true in the case of ANALYN as well, with some fine tuning required to obtain the desired results. A correction strategy dependent on the applied contact force and the separation may possibly improve the results [21]. Figure 8 presents the relative comparison of the contact area for a range of Δy values to the CONTACT results, emphasising the improvement using the new method as compared to existing fast approaches.

3.3. Computational cost

To make a representative comparison of the computational cost, MIM-1D is tested for different mesh sizes using the Hertzian profile against the other complete numerical methods i.e. Kalker's CONTACT, and the classical matrix inversion method (MIM) implemented as Matlab function. These comparisons are made using a 64 bits 2.70 GHz Intel processor. Only the computation time for the normal contact problem is considered. The time for CONTACT is taken from the generated output file, while the other two methods are measured using the elapsed CPU time averaged over a finite number of runs. These results are tabulated in Table 1. The gain in the computation speed using the new method with respect to the classical MIM is clear, with up to a 1000-fold speed up in cases where a comparison is possible. The conventional desktop employed is in fact unable to supply enough memory to carry out the simulations when using the fine meshes with MIM. CONTACT uses a bound-constrained conjugate gradient (BCCG) method with a fast Fourier transform (FFT) pre-conditioner which permits quicker resolution, even with a very fine discretisation [28]. The MIM-1D implementation here simply employs Matlab's inbuilt direct solver yet permits a significant gain in runtime, in no small part due to the reduced semi-analytical formulation of the method.

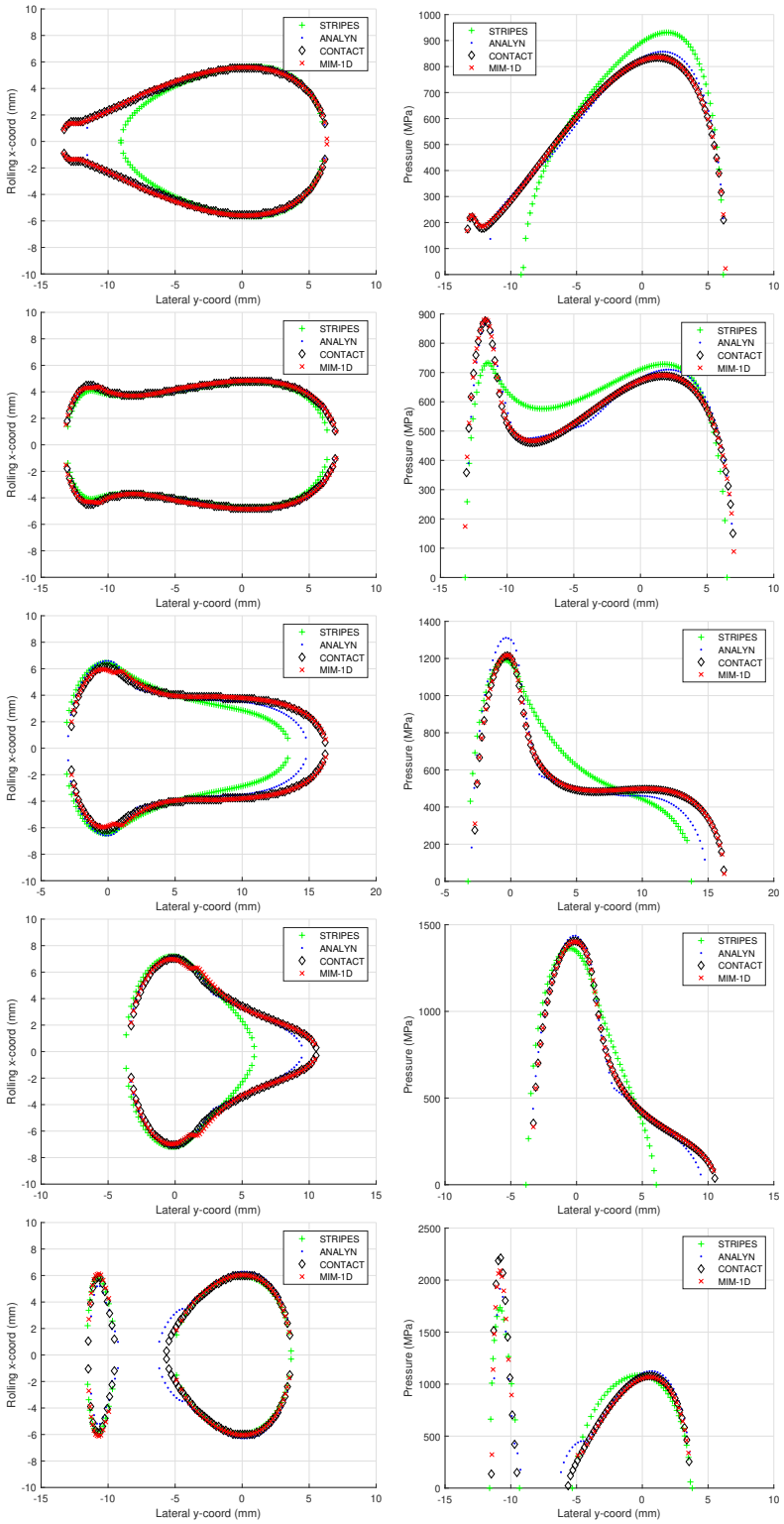

Figure 7. Contact patch (left), and the maximum pressure distribution $p_0(y)$ (right) for wheel-rail contact cases (from top to bottom): (a) $\Delta y = -1$ mm, (b) $\Delta y = 0$ mm, (c) $\Delta y = 1$ mm, (d) $\Delta y = 2$ mm, and (e) $\Delta y = 5$ mm.

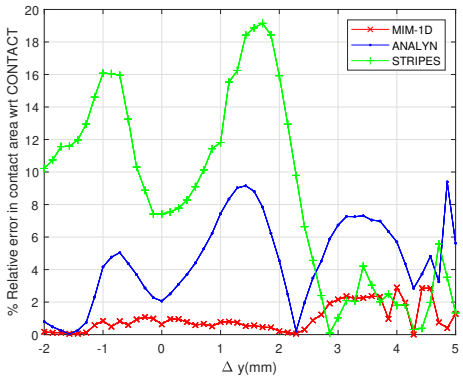

Figure 8. Comparison of the relative error in the contact area with reference results from CONTACT

Table 1. Comparison of CPU time with existing numerical approaches

	n	Time (s)		
Mesh size (mm)	Number of elements[a]	MIM	CONTACT	MIM-1D
0.2	51	1.002	0.1	0.010
0.1	101	40.28	0.2	0.037
0.02	501	$\gg$	5.2	0.342
0.01	1001	$\gg$	14.2	1.111

[a]The total number of elements in the case of MIM and CONTACT is $n \times n$.

4. Conclusion

A simplified boundary element formulation is presented in this paper and tested against two existing approximate methods, and a complete numerical method used as the reference. In essence, this approach further develops the discretisation strategy presented in [11], by using a semi-analytical methodology to determine the contact patch dimension in the rolling direction. The novel method, implemented in the algorithm MIM-1D, provides a precise approach comparable to more rigorous complete methods such as CONTACT, with lesser computing effort. The results from the theoretical and wheel-rail test cases presented allow the following conclusions to be drawn:

- The proposed approach MIM-1D enables an improved approximation of the pressure distribution and the contact area as compared to the other existing virtual penetration [15] and approximate surface deformation [21] methods.
- Comparison with a complete numerical method for wheel-rail contact shows close agreement, with the relative error in the contact area as compared to the reference results being less than 3% in all the tested cases using theoretical and wheel-rail profiles.
- The reduction in the number of system unknowns as compared to CONTACT due to a semi-analytical approach provides up to a 10-fold speed up with the current Matlab implementation. This should ideally improve further by using a programming language closer to machine language such as Fortran. Similarly, optimisation with respect to the iterative solver used should make the algorithm run faster.

It is important to keep in context that the latest versions of CONTACT incorporate

advanced numerical techniques to enable faster solving of the normal contact problem [28]. Incorporating similar numerical optimisation strategies may permit further improvement in the performance of MIM-1D as well. Further developments must also be implemented in order to accurately treat the flange contact, where the contact angle varies significantly in a small zone, thus violating the half-space assumption. These improvements are currently under study, within the scope of the implementation of MIM-1D in the dynamic multi-body simulation code VOCO (VOitures en COurbe). The eventual implementation should account for the coupling with the tangential contact problem, while taking the effect of friction into account. With proper optimisation, solving the classical normal contact problem using only strip elements should enable MIM-1D to be used as a good reference for other coarse models commonly employed in dynamic vehicle simulations.

Funding

The authors would like to thank Association Nationale de la Recherche et de la Technologie (ANRT), and ESI Group (France) for their financial support.

References

[1] Kalker JJ. Survey of wheel—rail rolling contact theory. Vehicle System Dynamics. 1979; 8(4):317–358.
[2] Piotrowski J, Chollet H. Wheel–rail contact models for vehicle system dynamics including multi-point contact. Vehicle System Dynamics. 2005;43(6-7):455–483.
[3] Knothe K. History of wheel/rail contact mechanics: from Redtenbacher to Kalker. Vehicle System Dynamics. 2008;46(1-2):9–26.
[4] Meymand SZ, Keylin A, Ahmadian M. A survey of wheel–rail contact models for rail vehicles. Vehicle System Dynamics. 2016;54(3):386–428.
[5] Hertz H. Über die Berührung fester elastischer Körper. Journal für die reine und angewandte Mathematik. 1882;92:156–171.
[6] Zhao X, Li Z. The solution of frictional wheel–rail rolling contact with a 3d transient finite element model: Validation and error analysis. Wear. 2011;271(1):444 – 452. Proceedings of the 8th International Conference on Contact Mechanics and Wear of Rail / Wheel Systems, Florence, 2009.
[7] Toumi M, Chollet H, Yin H. Finite element analysis of the frictional wheel-rail rolling contact using explicit and implicit methods. Wear. 2016;366-367:157 – 166. Contact Mechanics and Wear of Rail / Wheel Systems, CM2015, August 2015.
[8] Chouly F, Fabre M, Hild P, et al. An overview of recent results on Nitsche's method for contact problems. In: Bordas SPA, Burman E, Larson MG, et al., editors. Geometrically Unfitted Finite Element Methods and Applications; Cham. Springer International Publishing; 2017. p. 93–141.
[9] Kalker JJ. Rolling contact phenomena: Linear elasticity. In: Jacobson B, Kalker JJ, editors. Rolling Contact Phenomena; Vienna. Springer Vienna; 2000. p. 1–84.
[10] Vollebregt E. User guide for CONTACT, rolling and sliding contact with friction. Technical report 20-01, version "v20.2". Vtech CMCC; 2020.
[11] Knothe K, Le The H. A contribution to the calculation of the contact stress distribution between two elastic bodies of revolution with non-elliptical contact area. Computers & Structures. 1984;18(6):1025 – 1033.
[12] Johnson KL. Contact mechanics. Cambridge University Press; 1985.

[13] Linder C. Verschleiss von eisenbahnrädern mit unrundheiten [dissertation]. Zürich: ETH Zurich; 1997. Nr. 12342.
[14] Piotrowski J, Kik W. A simplified model of wheel/rail contact mechanics for non-Hertzian problems and its application in rail vehicle dynamic simulations. Vehicle System Dynamics. 2008 02;46:27–48.
[15] Ayasse JB, Chollet H. Determination of the wheel rail contact patch in semi-Hertzian conditions. Vehicle System Dynamics. 2005;43(3):161–172.
[16] Liu B, Bruni S, Vollebregt E. A non-Hertzian method for solving wheel–rail normal contact problem taking into account the effect of yaw. Vehicle System Dynamics. 2016;54(9):1226–1246.
[17] Sichani MS, Enblom R, Berg M. Comparison of non-elliptic contact models: Towards fast and accurate modelling of wheel–rail contact. Wear. 2014;314:111–117.
[18] Pascal JP, Sauvage G. The available methods to calculate the wheel/rail forces in non Hertzian contact patches and rail damaging. Vehicle System Dynamics. 1993;22(3-4):263–275.
[19] Ayasse JB, Chollet H, Maupu JL. Paramètres caractéristiques du contact roue-rail. INRETS report Nr. 225; 2000. ISBN 0768-9756.
[20] Pascal JP, Soua B. Solving conformal contacts using multi-Hertzian techniques. Vehicle System Dynamics. 2016;54(6):784–813.
[21] Sichani MS, Enblom R, Berg M. A novel method to model wheel–rail normal contact in vehicle dynamics simulation. Vehicle System Dynamics. 2014;52(12):1752–1764.
[22] Boussinesq J. Application des potentiels à l'étude de l'équilibre et du mouvement des solides élastiques. Gauthier-Villars; 1885.
[23] Cesbron J, Yin H, Anfosso-Lédée F, et al. Numerical and experimental study of multi-contact on an elastic half-space. International Journal of Mechanical Sciences. 2009; 51(1):33 – 40.
[24] Reusner H. Druckflächenbelastung und oberflächen-verschiebung im wälzkontakt von rotationskörpern [dissertation]. Germany: University of Karlsruhe; 1977.
[25] Love AEH. The stress produced in a semi-infinite solid by pressure on part of the boundary. Philosophical Transactions of the Royal Society of London Series A, Containing Papers of a Mathematical or Physical Character. 1929;228(659-669):377–420.
[26] Ayasse JB, Chollet H, Sebès M. Wheel-rail contact. In: Iwnicki S, Spiryagin M, Cole C, et al., editors. Handbook of railway vehicle dynamics, second edition. Chapter 7. Boca Raton: CRC Press/Taylor & Francis Group; 2019. p. 241–280.
[27] Quost X, Sebès M, Eddhahak A, et al. Assessment of a semi-Hertzian method for determination of wheel–rail contact patch. Vehicle System Dynamics. 2006;44(10):789–814.
[28] Vollebregt E. 100-fold speed-up of the normal contact problem and other recent developments in "CONTACT". 9th International Conference on Contact Mechanics and Wear of Rail/Wheel Systems, CM 2012. 2012 01;:79–86.

Appendix A. Solving the contact problem for the normal force N_i

The normal force acting on each strip N_i can be evaluated using Equation (15):

$$N_i = \pi a_i b_i p_{0_i}. \tag{A1}$$

The system of equations in matrix form is

$$\mathbf{u} = \mathbf{C'}\ \mathbf{N}, \tag{A2}$$

where $\mathbf{N} = \{N_1, ..., N_n\}^T$, and the matrix of influence coefficients $\mathbf{C'}$ is given by

$$\mathbf{C'} = \begin{bmatrix} (\pi a_1 b_1) C_{11} & \dots & (\pi a_n b_n) C_{1n} \\ \vdots & \ddots & \vdots \\ (\pi a_1 b_1) C_{n1} & \dots & (\pi a_n b_n) C_{nn} \end{bmatrix}. \tag{A3}$$

The half-length of the contact patch at the end of each iteration can be computed using

$$a_i = \left(\frac{1}{2E^\star} \frac{n_i m_i^2}{A_i + B_i} \frac{1}{b_i} N_i \right)^{\frac{1}{2}}. \tag{A4}$$

Equations (A2) and (A4) can subsequently be employed in the algorithm presented in Figure 3 to solve the contact problem.

Appendix B. Contact patch half-length a_i using ANALYN

The expression for the contact patch boundaries in ANALYN [21] is

$$a_i = \sqrt{\frac{d_i}{[1 + \alpha_i] A_i}}, \tag{B1}$$

where

$$d_i = \delta - [1 + \beta_i] h_i. \tag{B2}$$

Here, d_i is the penetration and the term $\beta_i h_i$ takes the surface deformation into account analytically as opposed to methods based on the virtual penetration where the deformation is neglected. The coefficients α_i and β_i are defined as:

$$\alpha_i = \frac{r_i}{m_i^2} \left(1 + \frac{B_i}{A_i} \right) - 1, \tag{B3}$$

$$\beta_i = \frac{r_i}{n_i^2} \left(1 + \frac{A_i}{B_i} \right) - 1, \tag{B4}$$

where A_i and B_i are the relative longitudinal and lateral curvatures respectively, while m_i, n_i, and r_i are non-dimensional Hertzian coefficients calculated using the local curvatures. The maximum pressure value p_{0_i} is

$$p_{0_i} = \frac{2E^*}{\pi} \frac{1}{n_i r_i} \frac{d_i}{a_i}. \tag{B5}$$

Squaring Equation (B1) and taking into account the expression for α_i, we have

$$d_i = \frac{r_i}{m_i^2} [A_i + B_i] a_i^2. \tag{B6}$$

Combining Equations (B5) and (B6), the half-length of the contact patch a_i can finally be written as

$$a_i = \frac{\pi}{2E^*} \frac{m_i^2 n_i}{A_i + B_i} p_{0_i}. \tag{B7}$$